Optics Communications 300 (2013) 17–21

Contents lists available at SciVerse ScienceDirect

Optics Communications

journal homepage: www.elsevier.com/locate/optcom

Multilayer graphene for Q-switched mode-locking operation in an erbium-doped fiber laser

Zhiteng Wang [a,1], Shou-En Zhu [b,1], Yu Chen [a], Man Wu [a], Chujun Zhao [a,*], Han Zhang [a,*], G.C.A.M. Janssen [b], Shuangchun Wen [a]

[a] Key Laboratory for Micro-/Nano-Optoelectronic Devices of Ministry of Education, College of Information Science and Engineering, Hunan University, Changsha 410082, China

[b] Micro & Nano Engineering Lab, Department of Precision and Microsystems Engineering, Delft University of Technology, Delft 2628CD, The Netherlands

ARTICLE INFO

Article history:
Received 29 January 2013
Received in revised form
11 March 2013
Accepted 12 March 2013
Available online 4 April 2013

Keywords:
Multilayer-graphene
Saturable absorber
Mode-locking
Q-switching
Erbium-doped fiber laser

ABSTRACT

We report the laser operation of Q-switched mode-locking (QML) in an erbium-doped fiber laser by using a multilayer graphene saturable absorber (SA), which consists of 22-layer of graphene fabricated by the chemical vapor deposition method. Based on our balanced twin detector measurement, the graphene sample is confirmed to show a saturable intensity of 3.375 MW/cm^2 and an absolute modulation depth of 40.27%. It is demonstrated that this graphene SA can readily produce high quality QML pulses. At the pump power of 391.9 mW, the stable mode-locked pulse train with the Q-switched envelope repetition rate of 16.98 kHz and the envelope width of 13.84 μs are achieved. The maximal main pulse peak power can reach up to 35.89 W. This verifies that the multilayer graphene can be still applied as an effective saturable absorber for passively Q-switched mode-locked operation.

1. Introduction

Laser mode-locking operation can be classified into the two types: continuous wave mode-locking (CWML), that is, mode-locked pulses emitted from every round trip show uniform pulse features, such as pulse duration, pulse energy, chirp and peak power [1]; Q-switched mode-locking (QML), that is, a train of pulses with cavity repetition rate inside a giant Q-switched envelope [2]. The repetition frequency of CWML is typically in the order of megahertz, which matches with the laser cavity repetition rate [1], whereas QML possesses two characteristic repetition frequencies: one relates with the cavity length and the other is the Q-switching modulation frequency in the kHz region [3]. Laser pulses generated from CWML show the advantages of high pulse stability and low noise. While, much higher pulse energy could be achieved by QML laser cavity [4]. Therefore, the QML pulses may be attractive in nonlinear frequency conversion, precise fabrication of microstructures [5], and surgery [6].

The scheme used for the generation of QML pulses can be active (e.g., exploiting acousto-optic modulator [7]) or passive (e.g., using saturable absorber (SA) [8]). Passively QML features a more compact geometry and simpler setup than active, which requires additional switching electronics (acousto-optic modulator) [7]. Doped bulk crystals [9], semiconductor SA mirrors (SESAMs) [10] and carbon nanotubes (CNTs) [11] are the common SAs in passive Q-switching. However, the doped crystals are mostly used in solid-state laser. The doped crystals, as SAs in fiber laser, require extra elements (mirrors, lenses) to focus the fiber output into the crystal. Therefore it is limited in a small range. SESAMs have limited operation bandwidth, typically few tens nm [12], which are not suitable for broad-band tunable pulse generation. Compared to SESAMs, CNTs can be considered as the broad-band SAs, operated on Yb-doped [13] and Er-doped [14] fiber laser. However, its operation wavelength is related to diameter and chirality of the CNTs [15].

Recently, graphene, a single layer of carbon in a hexagonal lattice, has been intensively researched due to its wonderful optical properties [16]. In laser photonics, graphene SA has been widely used as a broadband SA to passively Q-switch or mode lock the fiber laser or solid state laser, at different laser wavelengths ranging from 1 μm to 2 μm [17–28]. Conventional solitons [17–20], dissipative solitons [29], vector solitons [30], and Q-switched pulses [25,26] have been reported in fiber laser based on graphene SAs. In the present paper, we report on the QML pulses in a fiber laser cavity by using a multilayer graphene SA. The saturable intensity and the absolute modulation depth of the multilayer graphene SA is about 3.375 MW/cm^2 and 40.27%, respectively. Through a range of experiments with an erbium-doped fiber (EDF) laser, it has been demonstrated that this multilayer graphene SA

* Corresponding authors.
E-mail addresses: cjzhao@hnu.edu.cn (C. Zhao), hanzhang@hnu.edu.cn (H. Zhang).

[1] These authors contributed equally to this work.

0030-4018/$ - see front matter Crown Copyright © 2013 Published by Elsevier B.V. All rights reserved.
http://dx.doi.org/10.1016/j.optcom.2013.03.010

can readily produce high quality QML pulses. The stable mode-locked pulse train with envelope repetition rate of 16.98 kHz can be achieved. By fitting the Q-switched envelopes, we estimate that the minimal envelope width is about 13.84 μs and the maximal peak power of the main pulse is up to 35.89 W.

2. Characterization of the graphene samples

The graphene samples have been prepared by chemical vapor deposition, which had been detailed described in [31]. Firstly, a 3 inch SiO_2/Si substrate, coated with 300 nm Ni, was loaded into a tubular quartz tube and then heated up to 1000 °C with flowing H_2 and Ar. After flowing reaction gas mixtures (CH_4: H_2: Ar=250: 325: 1000 sccm) for ~5 min, the sample was rapidly cooled down to room temperature in order to completely stop the growth process. Since that average layer number of graphene on a Ni catalyst sensitively depends on the reaction time and cooling rate, one can control the layer number by those two experiment factors. In order to separate the fabricated graphene and substrate, one has to soak the as-prepared graphene/metal sample into BOE (buffered oxide etchant) solution to remove SiO_2 layer, then transfer floating graphene film to $FeCl_3$ solution in order to remove metal layer. The released graphene layer was freshened by DI (de-ionized) water few times. By dipping the targeted substrate into the water, one is able to "fish" the floating graphene film by the other substrate. In this paper, the graphene film was transferred onto the facet of optical fiber ferrule, and then the optical ferrule with the transferred graphene film was connected with another one. They were fused into the fiber laser as a graphene saturable absorber component.

Fig. 1(a) and (b) shows the atomic force microscopy (AFM) image and Raman spectrum of transferred multilayer graphene films, respectively. The D peak (1350 cm^{-1}) corresponds to the E_{2g} phonon at the Brillouin zone center. The G peak (1580 cm^{-1}) is caused by the breathing modes of sp^2 rings and together with a defect to active by double resonance [32]. The 2D peak (2700 cm^{-1}) is the second order of the D peak. An increase in the number of defects in graphene would result in an increase of the D-band intensity. In this case, the high ratio between the intensity of G peak and D peak implies that as-produced graphene sample possesses a low defect-level [32]. The 2D peak is always visible, even when no D peak is present, since no defects are required for the activation of two phonons with the same momentum, one backscattering from the other [32]. Multilayer graphene is identified by G/2D intensity ratio larger than 1 [33]. Moreover, the multilayer graphene is not uniform in thickness, as shown in Fig. 1(a). The optical transmittance of the multilayer graphene is 49.5% at 550 nm wavelength. This corresponding to an average numbers of 22 graphene layers according to the results of Nair et al. [34].

We characterized the saturable absorber performances of the multiplayer graphene film by nonlinear optical measurements, as shown in Fig. 1(d). This is a typical balanced twin detector measurement technology with details as follows. The laser source with operation wavelength at 1570 nm was used as input pulse with pulse width of 1.62 ps and repetition rate of 22.6 MHz. The maximal output power of the laser source is 30 mW. After the incident light passed through a tunable attenuation (OC-20B), the output light was divided into two equal laser beams by a 3-dB coupler. In the following, one laser beam propagated through the graphene SA, which was then measured by the photodiode detector A (918D/918L), while the other laser beam was directly connected with another photodiode detector B (918D/918L). In order to sufficiently suppress the possible detection error, these two detectors were connected to a power meter (2936-C) set

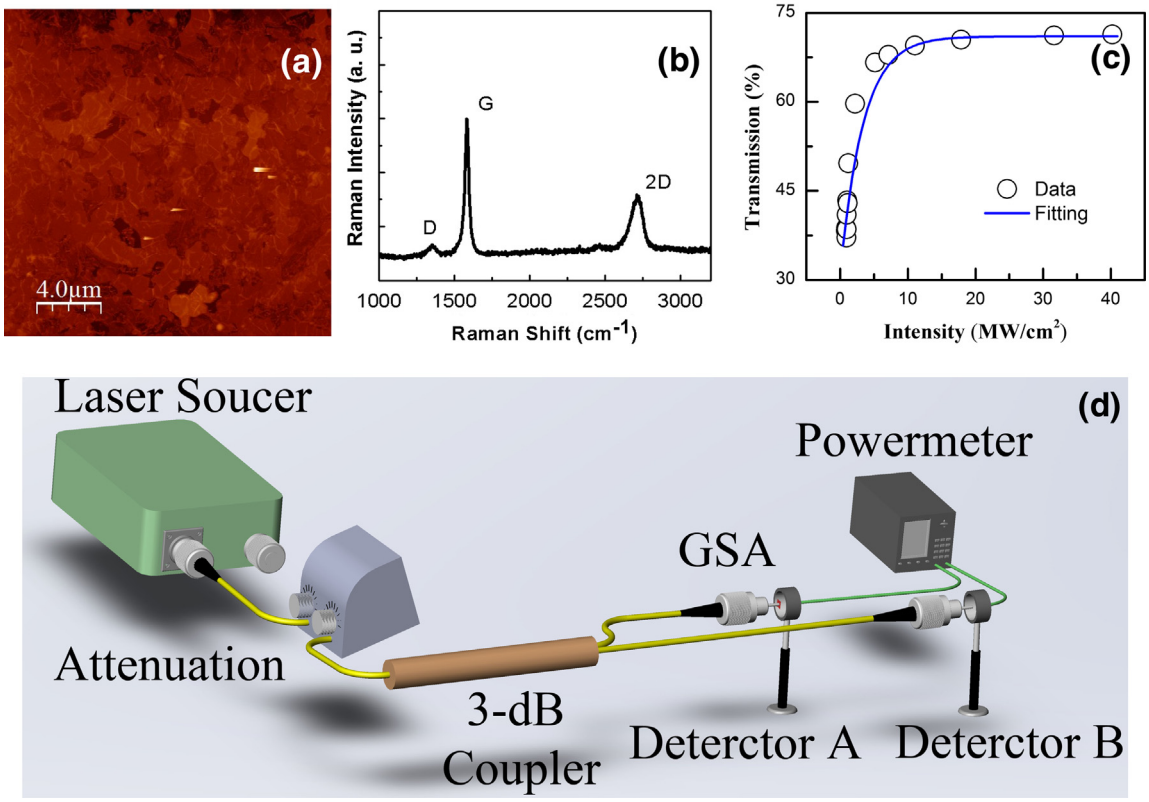

Fig. 1. (a) AFM image. (b) Raman spectrum. (c) Nonlinear transmission curve. (d) Nonlinear optical measurements setup of transferred multilayer graphene films. GSA: graphene saturable absorber.

by the same detection parameters, including the integration time and the detection wavelength. By continuously adjusting the attenuator loss, which corresponds to the variation of the input laser intensity, a series of output power and input power could be recorded. Upon the division of the output power by the input power, one yields the optical transmittance under different input powers.

The nonlinear transmission curve is plotted in Fig. 1(c). By fitting the experiment data with the equation $T(I) = 1 - \Delta T * \exp(-I/I_{sat}) - T_{NS}$, one can obtain the saturable intensity $I_{sat} = 3.375$ MW/cm^2 and the absolute modulation depth $\Delta T = 40.27\%$. The modulation depth of graphene saturable absorber is quite different from that reported by Huang et al. [28]. Despite that the graphene had been made by similar CVD method, the measured saturable absorption parameter can be different owing to some doping effects during the fabrication process and transfer process.

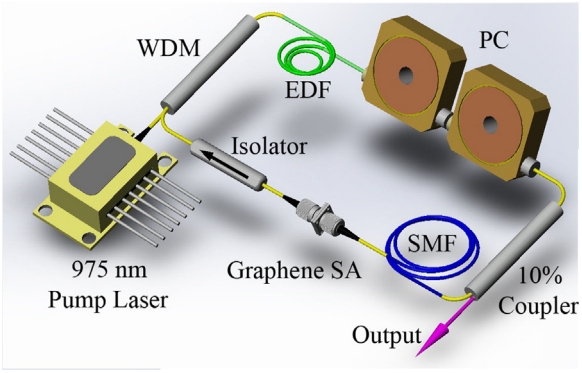

Fig. 2. The experimental setup of QML erbium-doped fiber ring laser mode-locked by multilayer graphene SA. WDM: wavelength-division-multiplexer; EDF: erbium-doped fiber; SMF: singer mode fiber; PC: polarization controller.

3. Experiment setup

Fig. 2 shows the experiment setup of an erbium-doped fiber ring laser mode-locked by the multilayer graphene SA. A piece of highly-doped erbium-doped fiber (EDF, LIEKKIEr80-8/125) with a length of 1.1 m and a group velocity dispersion 15 ps/km/nm at 1550 nm and peak absorption 80 dB/m at 1530 nm is used as the gain medium. The rest is 50 m-long single mode fiber (SMF) with group velocity dispersion 18 ps/km/nm at 1550 nm. A polarization-independent isolator (PII) is used as an isolator to ensure unidirectional light propagation. The polarization controller (PC) is employed to fine-tune the linear cavity birefringence. The total cavity length is 58.5 m, including several pieces of passive fibers for connecting the components, and the total cavity dispersion is estimated about -1.36 ps^2. A 980/1550 nm wavelength-division multiplexer (WDM) is used to launch the pumped light into the laser cavity. A 10% coupler is employed to couple out light. The laser is pumped by a 975 nm ALD98-500-B-FA diode laser. The output light is analyzed by an optical spectrum analyzer (AQ-6315A), a 500 MHz oscilloscope (TDS3054B) and a photo-detector.

4. Experimental results

The QML state is obtained at a pump power of 216.2 mW, as shown in Fig. 3. The Q-switched envelope fitting curves were obtained through the use of Eq. (1) in Ref. [9]. By fitting the Q-switched envelope, the envelope width is 21.23 μs. The interval between two envelopes is 82.7 μs, indicating that the repetition rate of the Q-switched envelopes is 12.08 kHz, as shown in Fig. 3(a).

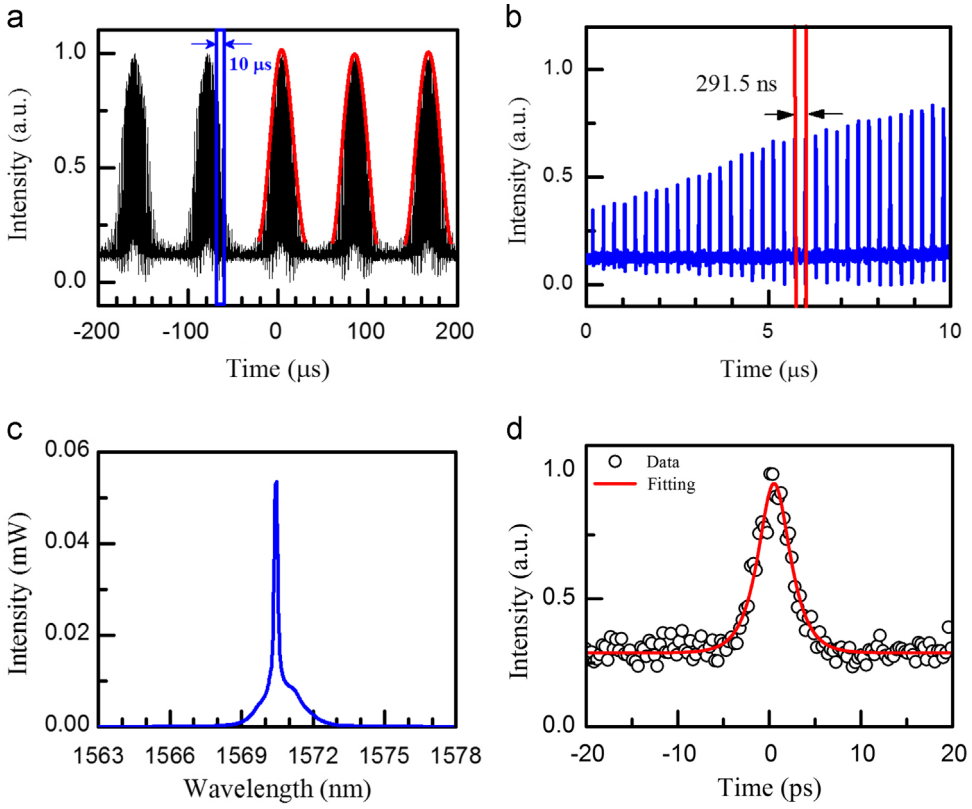

Fig. 3. The output Q-switched mode-locked pulses with pump power of 216.2 mW. (a) The oscilloscope trace (40 μs/div). (b) The pulse trace (1 μs/div). (c) The corresponding optical spectrum. (d) The measured autocorrelation trace and fitted curve by Sech^2 function.

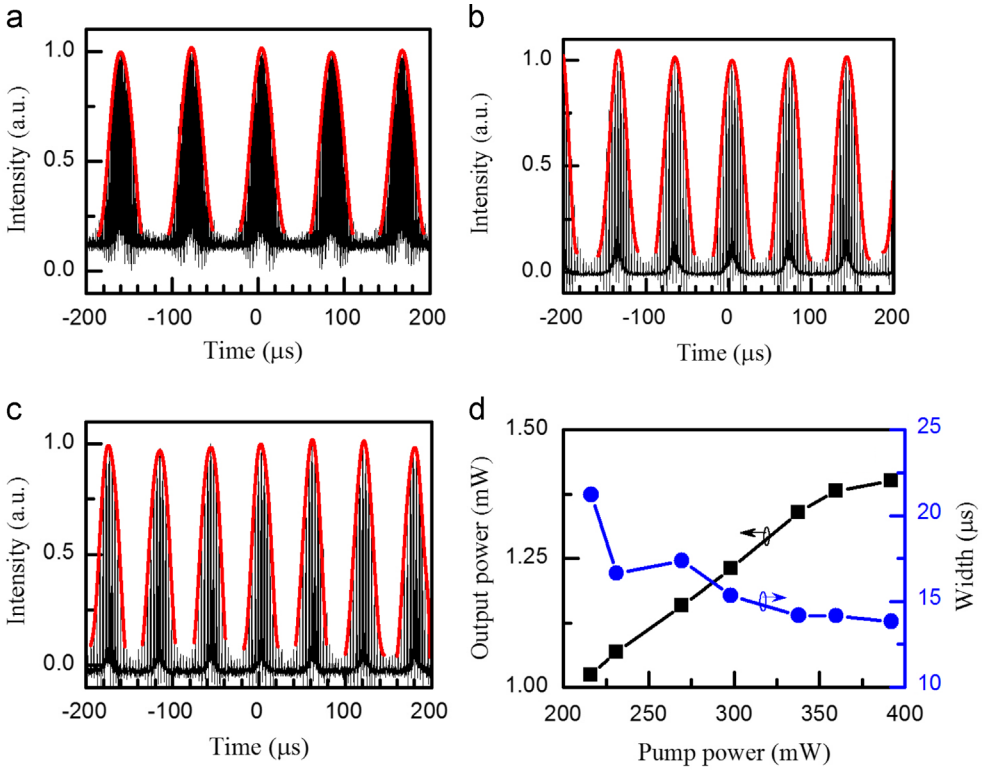

Fig. 4. (a), (b) and (c) The oscilloscope traces of the QML pulse trains under pump power of 216.2 mW, 269.4 mW and 359.7 mW, respectively. (d) The output power and envelope width the QML pulse trains under different input powers.

By zooming in the oscilloscope trace, its fine structure can be identified and we find a train of laser pulses inside the Q-switching envelope. The inter-pulse time interval is 291.5 ns. The central wavelength of the QML pulses is 1570.45 nm with 3-dB bandwidth of 0.20 nm, as shown in Fig. 3(c). No sideband has been seen in the optical spectrum. Correspondingly, the measured autocorrelation (AC) trace, shown in Fig. 3(d), is fitted by hyperbolic secant function with 3.75 ps full width at half maximum (FWHM), indicating that the real pulse width is 2.43 ps obtained by multiplying the autocorrelation trace width with the de-convolution factor, which is 0.648 for hyperbolic secant pulse shape.

Under the different pump power, the envelope repetition rate of the Q-switched mode-locked EDFL can be tuned from 12.08 kHz to 16.98 kHz by varying the pump power from 216.2 mW to 391.9 mW. The typical oscilloscope traces of the Q-switched pulse trains with the repetition rate of 12.08 kHz, 14.39 kHz and 16.95 kHz are shown in Fig. 4(a), (b) and (c), respectively. Fig. 4 (d) shows the output power and the envelope widths under different pump power. The peak power of the main pulses within Q-switched envelopes is calculated by $P_p = P_0/(NR_{eq}T_0)$, where P_0 is the average output power, R_{eq} is the repetition rate of the Q-switched envelope, T_0 is the pulse width of the mode locking pulses, and N is the number of pulses within a Q-switched envelope [9] with the width of the Q-switched envelope dividing by the pulse interval 291.3 ns. The peak power of main pulse is 35.89 W with the pump power of 391.9 mW, which is 26 times greater than that reported in Ref. [2] by using cavity loss modulation. At every specific repetition rate and pump power, the QML operation of this fiber laser can operate stably for several hours.

5. Discussion

According to the theory developed by Okhotnikov and co-workers, the critical intra-cavity pulse energy (E_c) required for the stable operation of CML against QML should obey the criterion [4]

$$E_c = \sqrt{E_{sat,G} * E_{sat,A} * \Delta T} \quad (1)$$

If the intra-cavity pulse energy (E_i) is greater than E_c, one can obtain CWML operation; otherwise, only the QML is obtained [4]. Here, based on the saturable absorption parameters of the multilayer graphene SA, we are able to analyze the operation dynamics in our laser cavity. As estimated, the multilayer graphene SA possess $E_{sat,A} = 4.6825$ pJ and $\Delta T = 0.4027$, and the gain saturation energy is $E_{sat,G} = 10$ μJ [35]. Based on the values for $E_{sat,G}$, $E_{sat,A}$ and ΔT, the critical pulse energy is calculated to be 4.34 nJ. Under a pump power of 391.5 mW, the maximal output power and the cavity round-trip time are 1.4 mW and 291.5 ns, respectively, which leads to an intra-cavity pulse energy of 4.08 nJ, which is smaller than the critical pulse energy E_c: 4.34 nJ. This can explain why we are able to achieve the QML operation in our fiber laser system.

6. Conclusion

In conclusion, an erbium-doped fiber laser passively mode-locked by a multilayer graphene SA at QML operation regime, had been reported. Based on our experimental measurement on the nonlinear optics property of graphene SA, we are able to explain why the fiber laser cavity can operate in QML regime. This graphene SA is confirmed to readily produce high quality Q-switched, mode-locked pulses. In the QML operation, the maximal repetition rate and the minimal pulse width of Q-switched envelope are 16.98 kHz and 13.84 μs, respectively. The repetition rate increases with the pump power, while the pulse width decreases with the pump power. The available main pulse peak power reaches up to 35.89 W. Our finding reveals that the multilayer graphene SA can be exploited as a broadband passive Q-switcher for both fiber laser and solid-state laser.

Acknowledgment

This work is partially supported by the National Natural Science Foundation of China (Grant no. 61205125), Natural Science Foundation of Hunan province (Grant no. 10JJ2047) and Program for New Century Excellent Talents in University (Grant no. NCET 11-0135). This work is part of the research programme of the Foundation for Fundamental Research on Matter (FOM), which is part of The Netherlands Organization for Scientific Research (NWO).

References

[1] O. Svelto, Principles of Lasers, 5th ed., Springer Verlag, Berlin, 2010.
[2] Y.M. Chang, J. Lee, J.H. Lee, Optics Express 19 (2011) 26627.
[3] K. Yang, S. Zhao, G. Li, M. Li, D. Li, J. Wang, J. An, Optical Materials 29 (2007) 1153.
[4] C. Hönninger, R. Paschotta, F. Morier-Genoud, M. Moser, U. Keller, Journal of the Optical Society of America B 16 (1999) 46.
[5] J. Neev, L.B. Da Silva, M.D. Feit, M.D. Perry, A.M. Rubenchik, B.C. Stuart, IEEE Journal of Selected Topics in Quantum Electronics 2 (1996) 790.
[6] U. Keller, Nature 424 (2003) 831.
[7] J. Jabczynski, W. Zendzian, J. Kwiatkowski, Optics Express 14 (2006) 2184.
[8] Y.F. Chen, S. Tsai, IEEE Journal of Quantum Electronics 37 (2001) 580.
[9] J.H. Lin, H.R. Chen, H.H. Hsu, M.D. Wei, K.H. Lin, W.F. Hsieh, Optics Express 16 (2008) 16538.
[10] C. Theobald, M. Weitz, R. Knappe, R. Wallenstein, J. Lhuillier, Applied Physics B 92 (2008) 1.
[11] J. Lee, J. Koo, Y.M. Chang, P. Debnath, Y.W. Song, J.H. Lee, Journal of the Optical Society of America B 29 (2012) 1479.
[12] O. Okhotnikov, A. Grudinin, M. Pessa, New Journal of Physics 6 (2004) 177.
[13] J. Nicholson, R. Windeler, D. DiGiovanni, Optics Express 15 (2007) 9176.
[14] T.H. Wu, K. Kieu, N. Peyghambarian, R. Jones, Optics Express 19 (2011) 5313.
[15] L.M. Zhao, D.Y. Tang, H. Zhang, X. Wu, Q. Bao, K.P. Loh, Optics Letters 35 (2010) 3622.
[16] F. Bonaccorso, Z. Sun, T. Hasan, A.C. Ferrari, Nature Photonics 4 (2010) 611.
[17] Q. Bao, H. Zhang, Z. Ni, Y. Wang, L. Polavarapu, Z. Shen, Q.H. Xu, D. Tang, K. Loh, Nano Research 4 (2011) 297.
[18] D. Popa, Z. Sun, T. Hasan, F. Torrisi, F. Wang, A.C. Ferrari, Applied Physics Letters 98 (2011) 073106.
[19] A. Martinez, K. Fuse, S. Yamashita, Applied Physics Letters 99 (2011) 121107.
[20] Y. Chen, C. Zhao, Z. Wang, J. Song, H. Zhang, S. Wen, Optical Engineering 51 (2012) 084203.
[21] W.B. Cho, J.W. Kim, H.W. Lee, S. Bae, B.H. Hong, S.Y. Choi, I.H. Baek, K. Kim, D.I. Yeom, F. Rotermund, Optics Letters 36 (2011) 4089.
[22] Y.W. Song, S.Y. Jang, W.S. Han, M.K. Bae, Applied Physics Letters 96 (2010) 051122.
[23] J. Sotor, G. Sobon, K.M. Abramski, Optics Letters 37 (2012) 2166.
[24] H. Zhang, Q. Bao, D. Tang, L. Zhao, K. Loh, Applied Physics Letters 95 (2009) 141103.
[25] Z. Luo, M. Zhou, J. Weng, G. Huang, H. Xu, C. Ye, Z. Cai, Optics Letters 35 (2010) 3709.
[26] Z. Wang, Y. Chen, C. Zhao, H. Zhang, S. Wen, IEEE Photonics Journal 4 (2012) 869.
[27] J. Liu, S. Wu, Q.H. Yang, P. Wang, Optics Letters 36 (2011) 4008.
[28] P.L. Huang, S.C. Lin, C.Y. Yeh, H.H. Kuo, S.H. Huang, G.R. Lin, L.J. Li, C.Y. Su, W.H. Cheng, Optics Express 20 (2012) 2460.
[29] J.L. Xu, X.L. Li, Y.Z. Wu, X.P. Hao, J.L. He, K.J. Yang, Optics Letters 36 (2011) 1948.
[30] H. Zhang, D. Tang, L. Zhao, Q. Bao, K.P. Loh, Optics Communications 283 (2010) 3334.
[31] Y. Lee, S. Bae, H. Jang, S. Jang, S.E. Zhu, S.H. Sim, Y.I. Song, B.H. Hong, J.H. Ahn, Nano Letters 10 (2010) 490.
[32] M. Pimenta, G. Dresselhaus, M.S. Dresselhaus, L. Cancado, A. Jorio, R. Saito, Physical Chemistry Chemical Physics 9 (2007) 1276.
[33] A. Ferrari, J. Meyer, V. Scardaci, C. Casiraghi, M. Lazzeri, F. Mauri, S. Piscanec, D. Jiang, K. Novoselov, S. Roth, Physical Review Letters 97 (2006) 187401.
[34] R. Nair, P. Blake, A. Grigorenko, K. Novoselov, T. Booth, T. Stauber, N. Peres, A. Geim, Science 320 (2008) 1308.
[35] M. Jiang, M. Fermann, J. Jimenez, D. Harter, M. Dagenais, S. Fox, Y. Hu, Optics Letters 24 (1999) 1074.